Title
Cd doping effects in the heavy-fermion compounds Ce2MIn8 (M=Rh and Ir)

Journal
Physical Review B, 81(24)

ISSN
2469-9950

Authors
Adriano, C
Giles, C
Bittar, EM
et al.

Publication Date
2010-06-15

DOI
10.1103/physrevb.81.245115

Cd doping effects in the heavy-fermion compounds Ce_2MIn_8 (M=Rh and Ir)

C. Adriano,[1,*] C. Giles,[1] E. M. Bittar,[1] L. N. Coelho,[1] F. de Bergevin,[2] C. Mazzoli,[2] L. Paolasini,[2] W. Ratcliff,[3] R. Bindel,[3] J. W. Lynn,[3] Z. Fisk,[4] and P. G. Pagliuso[1]

[1]*Instituto de Física "Gleb Wataghin," Universidade Estadual de Campinas (UNICAMP), 13083-970 Campinas, SP, Brazil*

[2]*European Synchrotron Radiation Facility, BP 220, F-38043 Grenoble Cedex, France*

[3]*NIST Center for Neutron Research, National Institute of Standards and Technology, Gaithersburg, Maryland 20899, USA*

[4]*University of California, Irvine, California 92697-4574, USA*

(Received 22 December 2009; revised manuscript received 15 March 2010; published 15 June 2010)

Low-temperature magnetic properties of Cd-doped Ce_2MIn_8 (M=Rh and Ir) single crystals are investigated. Experiments of temperature-dependent magnetic-susceptibility, heat-capacity, and electrical-resistivity measurements revealed that Cd doping enhances the antiferromagnetic (AFM) ordering temperature from T_N =2.8 K (x=0) to T_N=4.8 K (x=0.21) for $Ce_2RhIn_{8-x}Cd_x$ and induces long-range AFM ordering with T_N =3.8 K (x=0.21) for $Ce_2IrIn_{8-x}Cd_x$. Additionally, x-ray and neutron magnetic scattering studies showed that Cd-doped samples present below T_N a commensurate antiferromagnetic structure with a propagation vector $\vec{\varepsilon}=(\frac{1}{2},\frac{1}{2},0)$. The resolved magnetic structures for both compounds indicate that the Cd doping tends to rotate the direction of the ordered magnetic moments toward the *ab* plane. This result suggests that the Cd doping affects the Ce^{3+} ground-state single-ion anisotropy modifying the crystalline electrical field (CEF) parameters at the Ce^{3+} site. Indications of CEF evolution induced by Cd doping were also found in the electrical-resistivity measurements. Comparisons between our results and the general effects of Cd doping on the related compounds $CeMIn_5$ (M=Co, Rh, and Ir) confirms the claims that the Cd doping induced electronic tuning is the main effect favoring AFM ordering in these compounds.

DOI: 10.1103/PhysRevB.81.245115 PACS number(s): 71.20.Lp, 71.27.+a, 75.25.−j, 75.50.Ee

I. INTRODUCTION

Ce_2MIn_8 (M=Rh,Ir) are heavy-fermion compounds that belong to the broader family Ce_nMIn_{3n+2} (M=Co,Rh,Ir; n =1,2) where the occurrence of unconventional superconductivity (USC) in various members has provided a great opportunity to further study the relationship between magnetism, USC, and crystal structure. For the heavy-fermion superconductors (HFS) in this family, USC is believed to be mediated by magnetic fluctuations[1,2] and their critical temperatures seem to be related to the dimensionality of their crystal structures.[2–5] In fact, they are tetragonal variants of the cubic $CeIn_3$ structure with a layer of MIn_2 introduced between n blocks of $CeIn_3$ along the c axis.[2,3]

Particularly interesting in this family is the tunability of their ground state (GS) by pressure and/or doping which leads to remarkable phase diagrams showing interplay among USC, antiferromagnetism (AFM) and the presence of quantum critical phenomena.[2–15] For instance, applied pressure induces a high-pressure superconducting phase in the ambient pressure AFM members of this family, n=1 (115) member $CeRhIn_5$ (T_N=3.8 K) and n=2 (218) member Ce_2RhIn_8 (T_N=2.8 K).[2,7,8] The under pressure properties of the single-layer member $CeRhIn_5$ were much more extensively studied. Not long ago, evidence for hidden AFM order inside the SC state has been found in $CeRhIn_5$ under pressure and magnetic field.[2] The importance of simultaneous spin and charge fluctuations associated with a quantum critical point (QCP) for the superconductivity in this material has been shown.[7]

Regarding the doping phase diagrams of the Ce_nMIn_{3n+2} (M=Co,Rh,Ir; n=1,2) compounds, again the 115 members have been the main focus of the reported studies in the literature. For example, the reports on the $CeRh_{1-x}(Co,Ir)_xIn_5$ phase diagrams[5,6] reveal coexistence between AFM and SC for a large range of x. Furthermore, the critical temperatures of the superconducting samples varies linearly with the c/a ratio of the lattice parameters of the compounds.[5] Many other chemical substitutions were made in the 115 materials to contribute to the understanding of the microscopic tuning parameter of their GS.[4,5,9–15] La doping on the Ce^{3+} site for AFM members of the family Ce_nMIn_{3n+2} (M=Co,Rh,Ir; n =1,2) were aimed to describe the suppression of the Néel temperature by dilution and the effect of dimensionality on the percolation AFM ordering.[4]

Indeed, more revealing doping studies were made by the substitution of In by Sn (Refs. 9–12 and 16) and Cd.[13–15] This is because In, Cd, and Sn are not isovalent while Sn has one more p electron than In and Cd has one p electron less, opposite electronic effects might be expected. However, it was found that both elements suppress the SC state in $CeMIn_5$ for M=Co and Ir while Cd substitution tends to favor AFM ordering but Sn doping leads to its suppression.[10–15] The microscopic mechanisms of these doping that tune the GS in the $CeMIn_5$ compounds were attributed to the electronic tuning. It is therefore important and elucidative to explore the behavior for the other series in the Ce_nMIn_{3n+2} (M=Co,Rh,Ir; n=1,2) family and determine to what extent the same interpretation holds. In this regard, to study the n=2 member of the Ce_nMIn_{3n+2} family, the Ce_2MIn_8 could be particularly interesting since Cd and Sn doping are also possible in the 218's and they present an intermediate step in terms of dimensionality between the cubic $CeIn_3$ and the 115 compounds.[17,18]

Recently, interest in the 218 family has increased due to the discovery of the first HFS with a transition metal different from Co, Rh, or Ir, in the HF Ce_mMIn_{3m+2} family.

Ce_2PdIn_8 was found to be a new ambient pressure heavy-fermion SC ($T_c \sim 0.68$ K). It has not yet been established whether SC in this compound has an unconventional character or if it coexists with the magnetism on a microscopic scale.[19]

To further explore the microscopic effects of Cd doping in the Ce_nMIn_{3n+2} (M=Co, Rh, Ir; n=1, 2) family, we present in this paper the evolution of the low-temperature physical properties of the Ce_2MIn_8 (M=Rh, Ir) as a function of the Cd substitution. It is reported how the T_N=2.8 K and the magnetic structure [with $\vec{\varepsilon}=(\frac{1}{2},\frac{1}{2},0)$] (Ref. 20) of Ce_2RhIn_8 evolves as a function of Cd doping. Also the effects of Cd doping on the low-temperature spin-glass phase (T_g =0.6 K) (Ref. 21) of the HF Ce_2IrIn_8 are investigated. Our results are compared to those found for the Ce115's compounds and a discussion of the microscopic effect of the Cd in the GS of these systems is also given.

II. EXPERIMENTAL DETAILS

Single-crystalline samples of Ce_2MIn_8 (M=Rh, Ir) doped with Cd were grown from Indium flux in which various amounts of Cd were added to the flux[22,23] so that the nominal concentration of Cd can be defined by the Cd/In ratio used in the growth. We have performed prompt gamma neutron activation measurements at the instrument NG7 of the NIST Center for Neutron Research (NCNR) which reveal that the real Cd concentration in a given crystal is about 13% of the nominal concentration for samples of both series studied in this work. A detailed analysis of the actual Cd concentration in Cd-doped $CeMIn_5$ made by Pham *et al.*[13] showed that the Cd concentration in these crystals is approximately 10% of that in the flux from which they were grown. In this work, it will be used and labeled in the figures as the real Cd concentration measured by prompt gamma neutron activation.

The tetragonal ($P4/mmm$) structure and unit-cell parameters of all samples were determined by x-ray powder diffraction. Within the range of Cd concentrations studied, no appreciable changes in the lattice parameters due to the Cd doping were observed. Magnetization measurements as a function of the temperature were performed using a commercial superconducting quantum interference device in the temperature range between 2.0 and 300 K. Specific-heat and electrical-resistivity experiments were performed in a commercial physical properties measurement system in the temperature range between 0.3 and 10 K for the specific-heat measurements and between 1.9 and 300 K for the resistivity ones. The specific-heat setup uses a small mass calorimeter that employs a quasiadiabatic thermal relaxation technique while the electrical resistivity was measured using a low-frequency ac resistance bridge and four-contact configuration. The samples were screened and previously found to be free of surface contamination by residual In flux.

For the x-ray resonant magnetic scattering (XRMS) experiments, a selected crystal of Cd-doped Ce_2RhIn_8 with x =0.21 was prepared with polished (00l) flat surface, and approximately 3 mm×2 mm×1 mm. The mosaic spread of the sample was found to be $<0.05°$ by a rocking curve (θ scan) on a four-circle diffractometer. XRMS studies were performed at the ID-20 beamline at the European Synchrotron Radiation Facility (ESRF). The ID-20 x-ray source is a linear undulator with a 32 mm period. The main optical components are a double Si(111) crystal monochromator with sagittal focusing and two meridional focusing mirrors on either side of the monochromator. The sample was mounted on a cryostat (with a base temperature of 1.7 K using a Joule-Thomson stage), installed on a four-circle diffractometer with the a axis parallel to the beam direction. This configuration allowed σ-polarized incident photons in the sample. In a second run, the sample was mounted in a horizontal four-circle diffractometer with the (110) direction parallel to the beam direction and this configuration allowed π-polarized incident photons in the sample. During all measurements, we performed a polarization analysis, using LiF(220) crystal analyzer, appropriate for the energy of Ce L_2 absorption edge.

For the neutron magnetic scattering (NMS) experiments, selected crystals of Cd-doped Ce_2RhIn_8 and Ce_2IrIn_8, both with x=0.21 of Cd were prepared with sizes of approximately 4 mm×3 mm×1 mm. NMS measurements were carried out on BT-9 triple-axis neutron spectrometer of the NIST Center for Neutron Research (NCNR). The samples were cooled in an ILL orange cryostat (with a base temperature of 1.7 K), the horizontal collimators used were 40-47-40-80. Neutrons with incident energy E=35 meV were selected using the (002) reflection of a pyrolytic graphite monocromator, and filter to suppress the higher harmonics. Uncertainties where indicated are statistical in nature and represent one standard deviation.

III. RESULTS AND DISCUSSIONS

A. Macroscopic properties of $Ce_2(Rh,Ir)In_{8-x}Cd_x$

Figure 1 shows the temperature dependence in the low-T region of the magnetic susceptibility measured for a magnetic field H=0.1 T applied parallel $\chi_\parallel$ (closed symbols) and perpendicular $\chi_\perp$ (open symbols) to the c axis for pure (circles) and Cd-doped (a) Ce_2RhIn_8 and (b) Ce_2IrIn_8 single crystals with Cd concentrations of 0.03 (triangles) and 0.21 (squares). The inset in each panel shows the magnetic susceptibility as a function of the temperature from 2.0 to 300 K for the samples with x=0.21. The results in Fig. 1(a) for Cd-doped Ce_2RhIn_8 show AFM order for $T_N \approx 5.0$ K for x =0.21 of Cd and $T_N \approx 4.0$ K for x=0.03 of Cd. The results in Fig. 1(b) for Cd-doped Ce_2IrIn_8 show AFM order at T_N ≈ 3.8 K for x=0.21 and no magnetic order down to 2.0 K for x=0.03. For both materials, the magnetic susceptibility is larger for a field applied along the c axis, in agreement to what was found for the compounds in the In-based $R_mM_nIn_{3m+2n}$ (M=Co, Rh, or Ir, M=1, 2) series (except for R=Gd).[24–28] For the whole series, the susceptibility is anisotropic and the ratio $\chi_\parallel/\chi_\perp$ taken at T_N is mainly determined by the tetragonal crystalline electrical field (CEF) and reflects to some extent the CEF anisotropy. The ratio remains nearly constant as a function of Cd doping for each family, for example, for M=Rh the values of the ratio are roughly 1.6 and 1.5 for the samples with x=0.21 and 0.03, respectively. For M=Ir, the value of the ratio is nearly 2.2 and 2.1

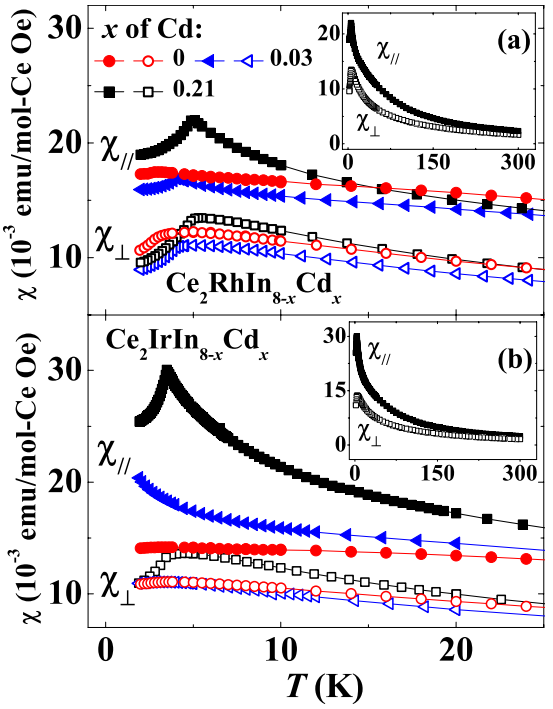

FIG. 1. (Color online) Temperature dependence of the magnetic susceptibility in the low-T region for Cd-doped (a) Ce_2RhIn_8 and (b) Ce_2IrIn_8 single crystals [pure compounds (circles), $x=0.03$ (triangles), and $x=0.21$ (squares)]. The magnetic field $H=0.1$ T was applied parallel $\chi_{\|}$ (closed symbols) and perpendicular $\chi_{\perp}$ (open symbols) to the c axis. The insets in both panels show the magnetic susceptibility as a function of the temperature from 2.0 to 300 K for $x=0.21$ of Cd in both systems. 1 emu/(mol Oe)$=4\pi\times10^{-6}$ m^3/mol.

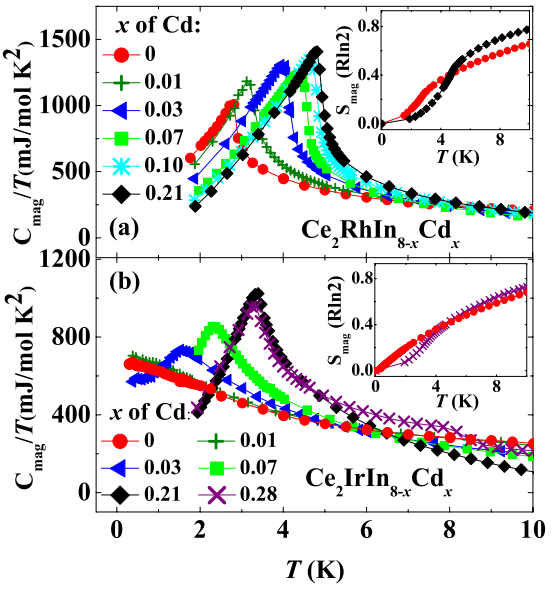

FIG. 2. (Color online) Magnetic specific-heat data ($C_{mag}=C_T-C_{latt}$) divided by temperature as a function of temperature for (a) $Ce_2RhIn_{8-x}Cd_x$ and (b) $Ce_2IrIn_{8-x}Cd_x$ single crystals for various Cd concentrations. The insets in each panels show the magnetic entropy S_{mag} for both systems.

for samples with $x=0.21$ and 0.03, respectively. Fits from the polycrystalline average of the magnetic-susceptibility data taken as $\chi_{poly}=(\chi_{\|}+2\chi_{\perp})/3$ for $T>150$ K using a Curie-Weiss law yield an effective magnetic moment $\mu_{eff}=2.48(8)\mu_B$ and a paramagnetic Curie-Weiss temperature $\theta_p=-44(1)$ K for $M=$Rh and $\mu_{eff}=2.51(6)\mu_B$ and $\theta_p=-42(1)$ K for $M=$Ir. The values of μ_{eff} and θ_p do not change significantly as a function of the Cd concentrations for both series in the range of concentration studied.

Figure 2 shows the Cd doping induced evolution of the low-temperature magnetic specific heat C_{mag} divided by temperature for (a) $Ce_2RhIn_{8-x}Cd_x$ and (b) $Ce_2IrIn_{8-x}Cd_x$ single crystals. To obtain the magnetic specific heat, the lattice specific-heat contribution (C_{latt}) was estimated from the specific-heat data of La_2RhIn_8 (not shown) and subtracted from the total specific heat (C_T) of each compound. The results of the specific-heat measurements for both series clearly show an enhancement of the AFM order as a function of Cd content in both systems. It is interesting to note that even for the samples with larger quantity of Cd, the phase-transition anomaly is still a sharp and well-defined peak, indicating a good quality of the crystals and a reasonably homogenous distribution of Cd concentration in the samples. More interesting is the case of $Ce_2IrIn_{8-x}Cd_x$ in which the spin-glass phase of the pure compound seems to evolve to a long-range AFM with increasing doping even though doping typically tends to increase disorder. This result suggests that the presence of a stronger Kondo effect in Ce_2IrIn_8 is relevant to the formation of the frustrated spin system in this compound.

The insets of both panels of Fig. 2 show the corresponding magnetic entropy per mole Ce for the pure and Cd-doped compounds in units of R ln 2. For $Ce_2RhIn_{8-x}Cd_x$, the recovered magnetic entropy for $x=0.21$ at 10 K is about $0.75R$ ln 2 (closed diamonds) that is a value larger than the recovered magnetic entropy seen for the pure compound ($0.65R$ ln 2, closed circles) at the same temperature. In the case of $Ce_2IrIn_{8-x}Cd_x$, the entropy of the Cd-doped sample is just slightly larger than the entropy of the pure compound. These results suggest the magnetic entropy is increasing as a function of the Cd concentration. On the other hand, the recovered magnetic entropies for these compounds still do not recover the R ln 2 value expected for the entropy of the ground-state doublet, suggesting the presence of partly compensated Kondo-ordered moments.

Figure 3 summarizes the temperature-doping phase diagrams resulting from heat-capacity measurements for $Ce_2MIn_{8-x}Cd_x$ (closed symbols), together with the results found by Pham *et al.*[13] for $CeMIn_5$ (open symbols) for $M=$Rh (squares) and Ir (circles). For $Ce_2RhIn_{8-x}Cd_x$, one can observe the evolution of the Néel temperature from 2.8 K for the pure compound to 4.8 K for $x=0.21$ of Cd. For higher Cd concentrations, T_N remains constant up to $x=0.35$. In this range of concentration, there seems to be a saturation of the Cd incorporation into the compound. For $Ce_2IrIn_{8-x}Cd_x$, one can observe that a Cd concentrations about $x=0.03$ already favors the establishment of long-range AFM order when the undoped[21] compound is a spin glass. The maximum value of T_N for $M=$Ir is 3.8 K for $x=0.21$ of Cd. For higher x, again a saturation of the Cd incorporation in samples is observed.

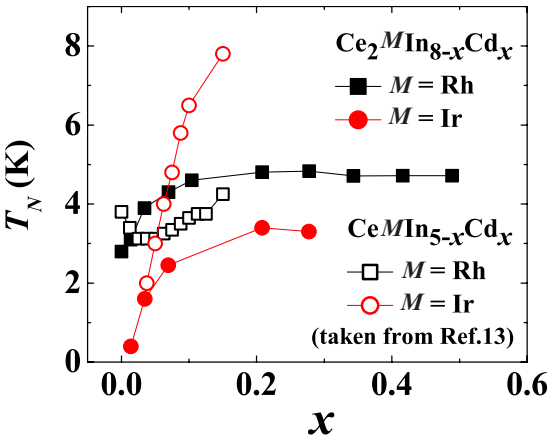

FIG. 3. (Color online) T_N as a function of Cd concentration for $Ce_2MIn_{8-x}Cd_x$ (closed symbols) and $CeMIn_{5-x}Cd_x$ (open symbols) for M=Rh (squares) and Ir (circles). The 115's results were taken from Ref. 13 for comparison.

Therefore, the results of Fig. 3 reveal that Cd doping favors AFM ordering in both $CeMIn_5$ (Ref. 13) and Ce_2MIn_8 (M=Rh,Ir) HF families. To further compare our results with those found by Pham *et al.*[13] for Cd-doped Ce115, we notice that, for $CeRhIn_5$, the Cd doping first reduces the T_N from 3.8 K for undoped material to 3.0 K, with a flat minimum for Cd concentration between 0.05 and 0.10. Higher Cd concentrations lead to a Néel temperature increase up to 4.2 K for $x \sim 0.15$. This behavior in Cd-doped $CeRhIn_5$ was suggested to be connected with an incommensurate to commensurate magnetic ordering evolution that can be induced by Cd doping in $CeRhIn_5$.[13] In Cd-doped Ce_2RhIn_8, we found that T_N is always increasing with the Cd concentration. The fact that pure Ce_2RhIn_8 already shows just below T_N=2.8 K a commensurate magnetic structure [with $\vec{\varepsilon}=(\frac{1}{2},\frac{1}{2},0)$] (Ref. 20) may explain the difference between the two structures.

For $CeIrIn_5$, the Cd doping initially suppress the superconductor state and for concentrations larger than 0.08, the AFM state appear and the increase in Cd content results in an increase in T_N from 2.0 K to around 8.0 K for x=0.15. In the case of Cd-doped Ce_2IrIn_8, we found that the spin-glass state of the pure compound evolves to a long-range AFM state and T_N also increases as a function of x but the maximum $T_N \sim 3.8$ K achieved is smaller than the one found for Cd-doped $CeIrIn_5$.[13]

The favoring of AFM in the Cd-doped 115's was interpreted using a Doniach-type scenario[29] where the Cd is inducing a decrease in the local density of states at the Ce^{3+} site which tends to reduce the Kondo effect favoring the AFM ordering.[13] The behavior of T_N found here for the Cd-doped 218 compounds corroborates to this interpretation since the same Cd doping effect would be expected to happen.

The temperature dependence in the low-T region of the electrical resistivity $\rho(T)$ is plotted in Fig. 4 panel (a) for M=Rh and Cd concentrations of x=0.03 (triangles) and 0.21 (diamonds), and panel (b) for M=Ir and Cd concentrations of 0.07 (squares) and 0.21 (diamonds). The insets in Figs. 4(a) and 4(b) show the behavior of the electrical resistivity for the entire range of temperatures for the samples with x

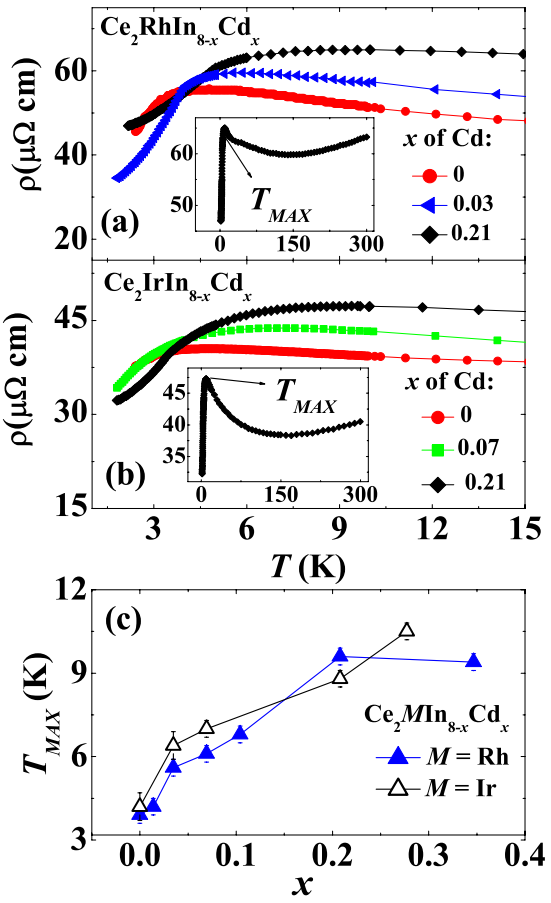

FIG. 4. (Color online) Temperature dependence of the electrical resistivity $\rho(T)$ in the low-T region for (a) $Ce_2RhIn_{8-x}Cd_x$ and (b) $Ce_2IrIn_{8-x}Cd_x$ compounds. The insets in each panels show $\rho(T)$ from 2.0 to 300 K for x=0.21 for both series. The arrows indicate the temperature T_{MAX} where the electrical resistivity has a maximum; (c) T_{MAX} as a function of the Cd concentration

=0.21 of Cd for both systems. For all crystals of the two series, the room-temperature value of the electrical resistivity is between 40 and 80 $\mu\Omega$ cm. Their high-temperature data show a weak metallic behavior down to 150 K, then the resistivity increases reaching a well-defined maximum at a temperature T_{MAX}, around 5.0–10 K [insets of the panels (a) and (b)]. The value of T_{MAX} from the resistivity measurements for all compounds as a function of the Cd content is plotted in Fig. 4(c) for $Ce_2RhIn_{8-x}Cd_x$ (closed triangles) and $Ce_2IrIn_{8-x}Cd_x$ (open triangles).

The results of the resistivity at low-T in Fig. 4(a) for $Ce_2RhIn_{8-x}Cd_x$ are showing clear kinks around 2.8 K, 3.8 K, and 4.8 K for x=0, 0.03, and 0.21, respectively, in good agreement with the values obtained for specific-heat measurements for the same values of x. Also for Cd-doped Ce_2IrIn_8 in Fig. 4(b), one can observe the kink in the resistivity measurements for x=0.21. The other curves for pure and Cd-doped Ce_2IrIn_8 with x=0.07 do not show obvious kinks at T_N, perhaps because the AFM ordering has not yet become long range for these Cd concentrations. The residual resistivity of the single crystals of Cd-doped Ce_2MIn_8 (M=Rh,Ir) is roughly two orders of magnitude larger than the residual resistivity of the $CeMIn_5$ (M=Co,Rh,Ir) com-

pounds. This behavior is consistent with the typically larger chemical disorder of the 218 materials when compared to that of the 115 materials.[30,31]

The most prominent feature of the resistivity data is the evolution of T_{MAX}, which, as shown in Fig. 4(c), is increasing as a function of the Cd doping for both series. This behavior of T_{MAX} is not expected within the Doniach-type scenario used to interpret the behavior of T_N in these series.

From the point of view of the Doniach model, the decrease in a local density of states induced by Cd doping drives the system to be more magnetic, i.e., the Ruderman-Kittel-Kasuya-Yoshida (RKKY) interactions are been favored while the Kondo effect is decreased. Based on this model, the T_{MAX}, that is, related to the Kondo energy scale should shift to lower temperatures as a function of the Cd concentration, in contrast to the observed results. This suggests that the Cd doping may have a second effect that produces the increase in the maximum in the resistivity. To further understand the role of Cd substitution in Ce_2MIn_8, we have performed x-ray and neutron magnetic scattering experiments to determine the low-T magnetic structure with Cd doping.

B. Magnetic structure of $Ce_2(Rh,Ir)In_{7.79}Cd_{0.21}$

Cd doping perturbations in the AFM state were further explored through x-ray and neutron magnetic scattering experiments. For these experiments, we chose samples with the larger Néel temperature for both series with Cd concentration of $x=0.21$ and $T_N=4.8$ K and 3.8 K, respectively, to M =Rh and Ir.

The XRMS experiments were performed with the incident photon energy at the Ce L_2 absorption edge in resonant condition in order to enhance the small signal from the AFM order of Ce^{3+} ions below T_N, and polarization analysis was performed to more properly determine the moment direction. Magnetic peaks of the Cd-doped Ce_2RhIn_8 with $x=0.21$ were observed in dipolar resonant condition at temperatures below $T_N=4.8$ K at reciprocal-lattice points forbidden for charge scattering and consistent with an antiferromagnetic structure with propagation vector $(\frac{1}{2},\frac{1}{2},0)$.[32] This is the same propagation vector found by Bao *et al.*[20] for the pure compound, showing that Cd doping is not changing the propagation vector. This indicates that although the Cd doping enhances the magnitude of the average magnetic exchange between neighboring Ce^{3+} ions it does not affect the sign of the relative magnetic interaction between them.

Figure 5(a) displays the temperature dependence of the magnetic moment of the Ce^{3+} ion, which is proportional to the square root of the integrated intensities, of the $(\frac{1}{2},\frac{1}{2},9)$ magnetic reflection at an incident photon energy of 6164 eV (Ce L_2 edge) and measured in π-σ' polarization channel. A Voigt peak shape was used to fit transverse θ scans (sample rotation) through the reciprocal-lattice points in order to obtain the integrated intensities. The data were taken between $T=2.0$ K and $T=5.2$ K while warming the sample. The inset shows the experimental θ scans for two different temperatures, $T=4.6$ K (open triangles) and $T=2.0$ K (closed squares), where one can observe the decrease in the intensity

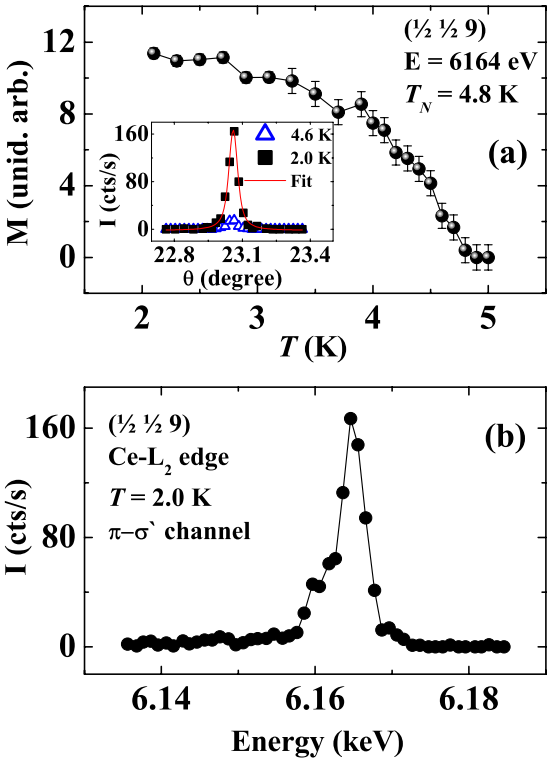

FIG. 5. (Color online) (a) Temperature dependence of the ordered magnetic moment, proportional to square root of the integrated intensity, of the $(\frac{1}{2},\frac{1}{2},9)$ magnetic reflection measured with transverse θ scans in the temperature range between $T=2.0$ and 5.2 K for $Ce_2RhIn_{7.79}Cd_{0.21}$. The inset shows two θ scans of the same reflection for different temperatures: 4.6 K (open triangles) and 2.0 K (closed squares). The continuous line is a Voigt fit to the observed data at $T=2.0$ K. (b) Energy line shape of the $(\frac{1}{2},\frac{1}{2},9)$ magnetic peak at $T=2.0$ K for π-σ' polarization channel at the Ce L_2 absorption edge. The line is just a guide to the eyes.

as T approaches T_N. The continuous line is a Voigt fit to the observed data at $T=2.0$ K and show the very good quality of the crystal with a full width at half maximum (FWHM) of 0.05°. The decrease in the intensities as the temperature is increased toward the bulk T_N demonstrates the magnetic character of this reflection, and is in very good agreement with the Néel temperature obtained from specific-heat measurements. The smooth decrease in the intensity through T_N is a signature of a second-order-type transition.

Figure 5(b) shows the energy dependence of the $(\frac{1}{2},\frac{1}{2},9)$ magnetic reflection around the Ce L_2 absorption edge at T =2.0 K. A resonant enhancement was observed at 1 eV above the absorption edges revealing a result consistent with a dominant electric dipolar character ($E1$) of this transition (from $2p$ to $5d$ states). These results confirm the magnetic origin of the $(\frac{1}{2},\frac{1}{2},l)$ reflections due to the existence of an antiferromagnetic structure doubled in the basal plane.

To completely determine the magnetic structure of the system, an important aspect is the orientation of the magnetic ordered moment with respect to the crystal lattice. While the magnetic wave vector gives the relative orientation between the neighboring spins, the direction of moment gives information about the magnetic anisotropy (e.g., CEF effects) of

the ordered spins. For collinear magnetic structures and polarized incident photons, the polarization dependence of the XRMS assumes a simple form for dipolar resonances, and the intensities of magnetic Bragg peaks are given by[33]

$$I \propto \frac{1}{\mu^* \sin(2\theta)} \left| \sum_n f_{nE1}^{XRES}(\vec{k},\hat{\epsilon},\vec{k}',\hat{\epsilon}',\hat{z}_n) e^{i\vec{Q}\cdot\vec{R}_n} \right|^2, \quad (1)$$

where μ^* is the absorption correction for asymmetric reflections, 2θ is the scattering angle, $\vec{Q}=\vec{k}'-\vec{k}$ is the wave-vector transfer, and $\vec{k}$ and $\vec{k}'$ ($\hat{\epsilon}$ and $\hat{\epsilon}'$) are the incident and scattered wave (polarization) vectors, respectively. $\vec{R}_n$ is the position of the nth resonant atom in the lattice, $e^{i\vec{Q}\cdot\vec{R}_n}$ is the magnetic structure factor, and finally $\hat{z}_n$ is the unit vector of the moment direction of the Ce^{3+} ions. The resonant scattering amplitude contains both dipole ($E1$) and quadrupole ($E2$) contributions. For the determination of the magnetic structure, we have used the second term of the electric dipole transition ($E1$) form factor (f_{nE1}^{XRES}) which can be written as

$$f_{nE1}^{XRES} \propto \begin{bmatrix} 0 & \hat{k}\cdot\hat{z}_n \\ -\hat{k}'\cdot\hat{z}_n & (\hat{k}\times\hat{k}')\cdot\hat{z}_n \end{bmatrix} \quad (2)$$

$$\propto \begin{bmatrix} 0 & z_1\cos\theta + z_3\sin\theta \\ -z_1\cos\theta + z_3\sin\theta & -z_2\sin(2\theta) \end{bmatrix}, \quad (3)$$

where θ is the Bragg angle and z_1, z_2, and z_3 are the components of the magnetic moment at the nth site, according to the commonly used geometry convention of Ref. 34. In this convention, each term of the matrix [Eq. (2)] represents one polarization channel: σ, π, σ', and π' describe the incident (nonprimed) and scattered (primed) photon polarizations. To describe the orientation of the magnetic moment, η is the angle of the moment with relation of the ab plane and ψ the angle in the ab plane.

The magnetic structure of $Ce_2RhIn_{7.79}Cd_{0.21}$ was resolved by comparing the intensities of the $(\frac{1}{2},\frac{1}{2},l)$ (with l=4, 5, 6, 7, 8, 9, and 10) magnetic reflections with those expected using the model given in Eqs. (1)–(3).[26,33,35–38] For this determination, we used the data obtained for (σ-π') polarization channel measured with σ incident photons in the energy of the Ce L_2 edge and T=2.0 K. For this channel, the component of the matrix used was the term $-\hat{k}'\cdot\hat{z}_n$ of the Eq. (2). Since the tetragonal structure of Cd-doped Ce_2RhIn_8 contains two magnetic Ce^{3+} ions per unit cell in the c direction, this implies that two possibilities of an AFM coupling can take place along the c axis: (1) sequence ++ or (2) sequence +−, where the symbols + and − represent the relative orientation of the magnetic moment of one Ce^{3+} ion with respect to the other. We checked the two sequences in our model and the sequence +− gives the better results, in agreement with the result obtained for pure Ce_2RhIn_8.[20]

The experimental intensities of the magnetic peaks $(\frac{1}{2},\frac{1}{2},l)$ for $Ce_2RhIn_{7.79}Cd_{0.21}$ are compared to the model discussed above and displayed in Fig. 6. The best fit (solid line in Fig. 6) using the model was obtained for $\eta=47°\pm3°$ and $\psi=45°\pm8°$.

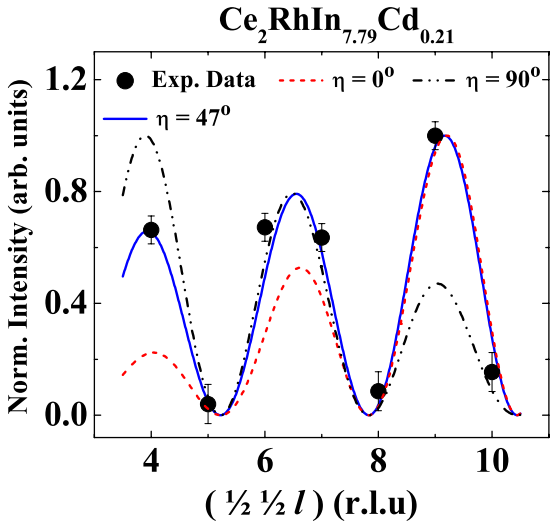

FIG. 6. (Color online) The l dependence (in reciprocal-lattice units) of the normalized intensities of the magnetic peaks $(\frac{1}{2},\frac{1}{2},l)$ measured at the energy of the Ce L_2 edge at T=2.0 K in the σ-π' polarization channel for $Ce_2RhIn_{7.79}Cd_{0.21}$. The solid line represents the best fit using the model discussed in Eqs. (1)–(3) for η=47° and ψ=45°. The other lines represent the model calculated for ψ=45° and η=0° (dashed line) and η=90° (dashed-dotted line).

The results in Fig. 6 completely determine the magnetic structure of the $Ce_2RhIn_{7.79}Cd_{0.21}$ sample. The magnetic-moment direction shows a slight evolution toward the basal plane when compared with the pure Ce_2RhIn_8 where the moment direction is tilted 52° from the basal plane. Those results indicate that Cd doping also subtly changes the single-ion anisotropy of the CEF GS which mainly determines the direction of the ordered moment. Analyzing these results in a more general way, one can compare our results with those found for the In-based $R_mM_nIn_{3m+2n}$ (M=Co, Rh, or Ir; M=1,2; R=rare earth) series. In a recent theoretical work using a mean-field model including an isotropic first-neighbors (RKKY) interaction and the tetragonal CEF,[25] it was demonstrated that, for realistic values of the interactions and CEF parameters, it is possible to determine qualitatively the direction of the ordered moments and the behavior of the ordering temperature for these series. Following the trend obtained for the In-based $R_mM_nIn_{3m+2n}$ when the Néel temperature of the tetragonal members is higher than the Néel temperature of the cubic relative, the magnetic-moment direction tends toward the c axis, considering dominant CEF effects. Therefore, although the Cd doping induces some changes in the CEF parameters, our results show that the direction of the ordered moment tend to rotate to the ab plane even with an increase in the T_N for a Cd-doped sample, strongly suggesting that the dominant effect to raise T_N in these systems is the electronic tuning induced by the Cd doping. The indication that the tetragonal CEF is changing as a function of Cd doping in these series may explain the behavior of T_{MAX} in electrical-resistivity measurements. If this subtle change in the CEF parameters leads to an increase in the energy level of the first excited doublet it may cause an increase in T_{MAX}. However, further experiments to obtain direct evidence of this change in CEF scheme as a function of Cd doping is necessary to confirm this claim.

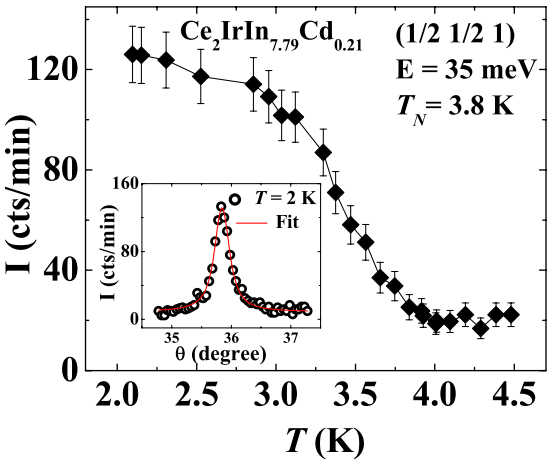

FIG. 7. (Color online) Temperature dependence of the integrated intensities of the $(\frac{1}{2},\frac{1}{2},1)$ magnetic reflection measured during heating the sample in the temperature range between $T=2.0$ K and $T=4.5$ K for $Ce_2IrIn_{7.79}Cd_{0.21}$ for 35 meV. The inset shows the θ scan of the same reflection for $T=2.0$ K for $Ce_2IrIn_{7.79}Cd_{0.21}$ where the continuous line is a Voigt fit to the observed data.

The NMS experiments were performed to study both Cd-doped Ce_2RhIn_8 and Ce_2IrIn_8 for $x=0.21$ of Cd concentration. The Rh member was studied by NMS to determine the effective magnetic moment of the Ce^{3+} ions in low T. The experiments were performed with an incident energy of 35 meV with no absorption corrections based on the fact that at 35 meV, the neutron penetration length is about 2.0 mm, which is larger than the thickness of the sample. Indeed, we measured rocking curves for different domains and no significant changes on the intensities were noticed. Magnetic peaks of the $Ce_2(Rh,Ir)In_{7.79}Cd_{0.21}$ were observed at temperatures below $T_N=4.8$ K and 3.8 K, respectively, for Rh and Ir samples, at reciprocal-lattice points forbidden for nuclear scattering and consistent with an antiferromagnetic structure with propagation vector $(\frac{1}{2},\frac{1}{2},0)$. These results show that the Cd-doped Ce_2IrIn_8 sample presents the same propagation vector found for pure and Cd-doped Ce_2RhIn_8 samples.

Figure 7 displays the temperature dependence of the integrated intensity of the $(\frac{1}{2},\frac{1}{2},1)$ magnetic reflection of the $Ce_2IrIn_{7.79}Cd_{0.21}$ compound, measured between $T=2.0$ K and $T=4.5$ K while warming the sample. The inset shows an experimental θ scan for $T=2.0$ K. The continuous line is a Voigt fit to the observed data at $T=2.0$ K and shows a FWHM of 0.2°, a value larger than the one obtained for x-ray diffraction because of the larger divergence of the neutron beam compared with x rays. The decrease in the intensity as the temperature is increased toward the bulk T_N indicates the magnetic character of this reflection, and is in very good agreement with the Néel temperature obtained from specific-heat measurements. The smooth decrease in the intensity is a signature of a second-order-type transition, found also for $Ce_2IrIn_{7.79}Cd_{0.21}$ sample.

To completely determine the magnetic structure of $Ce_2IrIn_{7.79}Cd_{0.21}$, it is necessary to determine the magnetic-moment orientation of the Ce^{3+} ion in relation to the crystallographic axis. Integrated intensities of magnetic Bragg peaks were determined using a Voigt fit in the θ scans. These magnetic peaks were first normalized using the structural Bragg peaks $(00l)$ for $l=1$, 2, 3, 4, and 7; $(11l)$ for $l=1$, 2, 3, 4, 5, and 6; and $(22l)$ for $l=0$, 1, 2, 3, and 6. In barn units, the magnetic cross section for a collinear magnetic structure using unpolarized neutrons is given by[20,39,40]

$$\sigma(Q)=\left(\frac{\gamma r_0}{2}\right)^2|S|^2|f(Q)|^2\sum_{\mu,\nu}(\delta_{\mu,\nu}-\hat{Q}_\mu\hat{Q}_\nu)F^*_\mu(Q)F_\nu(Q), \tag{4}$$

where $(\gamma r_0/2)^2=0.07265$ b/μ_B^2, S is the effective magnetic moment of the Ce^{3+} ion, $f(Q)$ is the Ce^{3+} magnetic form factor,[41] and $F_\mu(Q)$ is the μth cartesian component of magnetic structure factor per Ce_2IrIn_8. The calculations were made considering the average of the possible domains and the result is given by[20]

$$\sigma(Q)=\left(\frac{\gamma r_0}{2}\right)^2|S|^2|f(Q)|^2\langle 1-(\hat{Q}\cdot\hat{z_n})^2\rangle|F_S(Q)|^2, \tag{5}$$

where $F_M(Q)$ is the magnetic form factor calculated for the two Ce^{3+} ions of the unitary cell along the c axis, $\hat{z_n}$ is the unit vector of the magnetic moment, and the average, $\langle 1-(\hat{Q}\cdot\hat{z_n})^2\rangle$ is over the magnetic domains.[20]

The NMS technique does not allow the moment direction determination in the ab plane due to the square symmetry,[39,40] only the moment direction relative to the c axis is allowed. Considering the magnetic moment with an arbitrary orientation in relation to the c axis, there are in general 16 magnetic domains with tetragonal symmetry, for an equal population of domains, the average term of the Eq. (5) could be written as[20]

$$\langle 1-(\hat{Q}\cdot\hat{z_n})^2\rangle=1-\frac{\cos^2\alpha\cos^2\eta+2\sin^2\alpha\sin^2\eta}{2} \tag{6}$$

here α is the angle of $\vec{Q}$ in relation to the basal plane and η is the angle between the moment direction and the basal plane.

Figure 8 shows the l dependence of the experimental $(\frac{1}{2},\frac{1}{2},l)$ magnetic intensities compared with the magnetic cross section $\sigma(Q)$ in millibarn units calculated using the model discussed in Eqs. (4)–(6). The solid line in Fig. 8 displays the best fit obtained for $\eta=21°\pm5°$ and the ordered magnetic moment at 2.0 K was determined as $S=0.4(5)\mu_B$ per Ce. The model calculated for $\eta=0°$ is represented by the dashed line while the dashed-dotted line shows the model to $\eta=90°$.

The results in Fig. 8 completely determine the magnetic structure of $Ce_2IrIn_{7.79}Cd_{0.21}$ sample. The magnetic-moment direction of the doped compound shows a large evolution toward to the basal plane when compared with the $Ce_2RhIn_{7.79}Cd_{0.21}$ where the moment direction lies at 47° of the basal plane.

NMS experiments were performed also in $Ce_2RhIn_{7.79}Cd_{0.21}$ to complement the study made with XRMS and to determine the effective magnetic moment S of this compound in low-T. Table I shows the observed magnetic integrated intensities of the $(\frac{1}{2},\frac{1}{2},l)$ ($l=0$, 1, 2, 3, 4, 5,

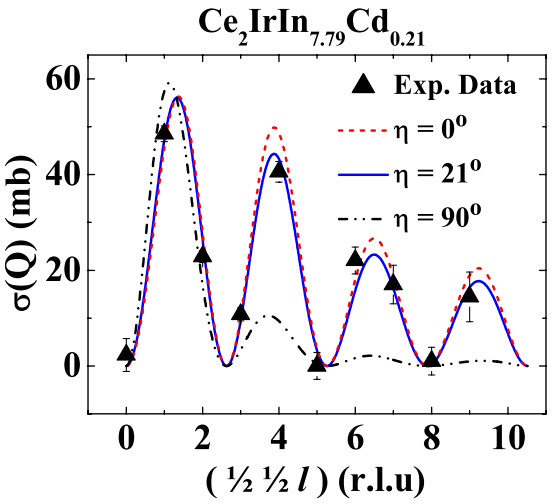

FIG. 8. (Color online) The l dependence (in reciprocal-lattice units) of the $\sigma(Q)$ of the magnetic peaks $(\frac{1}{2},\frac{1}{2},l)$ measured at the energy of 35 meV at $T=2$ K. The solid line represents the best fit using the model discussed in Eqs. (4)–(6) for $\eta=21°$ and $S=0.4(5)\mu_B$. The other lines represent the model calculated for $\eta=0°$ (dashed line) and $\eta=90°$ (dashed-dotted line).

6, and 7) magnetic reflections normalized by the nuclear peaks (00l) for $l=1$, 2, 3, 4, and 7; (11l) for $l=1$, 2, 3, 4, 5, and 6; and (22l) for $l=0$, 1, 2, 3, and 6; the theoretical cross section was calculated using Eqs. (4)–(6) and the best-fit data is $\eta=47(5)°$ and an ordered magnetic moment $S=0.9(2)\mu_B$. The result of the magnetic-moment direction found for $Ce_2RhIn_{7.79}Cd_{0.21}$ sample is in very good agreement with the result found by means of the XRMS, showing the consistency of the two experimental methods. The ordered magnetic moment for Ce^{3+} ion in low-T equal to $0.9(2)\mu_B$ that is a value larger than the value found for pure Ce_2RhIn_8, also consistently with the fact that Cd doping is favoring the AFM order in this system.

TABLE I. Magnetic Bragg intensities, σ_{obs}, (mb) observed at 1.6 K with $E=35$ meV. The theoretical intensities, σ_{calc} (mb), were calculated using Eqs. (4)–(6) with $\eta=47°$ and $S=0.9(2)\mu_B$ per Ce.

$\vec{Q}$	σ_{exp}	σ_{calc}
$(\frac{1}{2},\frac{1}{2},0)$	0.1(2)	0
$(\frac{1}{2},\frac{1}{2},1)$	138(2)	134
$(\frac{1}{2},\frac{1}{2},2)$	61(1)	56
$(\frac{1}{2},\frac{1}{2},3)$	21(1)	19
$(\frac{1}{2},\frac{1}{2},4)$	66(1)	69
$(\frac{1}{2},\frac{1}{2},5)$	3(2)	4
$(\frac{1}{2},\frac{1}{2},6)$	39(1)	30
$(\frac{1}{2},\frac{1}{2},7)$	38(1)	28

IV. CONCLUSIONS

The low-temperature physical properties of Cd-doped Ce_2MIn_8 (M=Rh,Ir) single-crystalline samples have been investigated. The results of the susceptibility, heat capacity, and resistivity as a function of temperature revealed an enhancement of the Néel temperature from 2.8 K for the pure compound to 4.8 K for the Cd-doped sample for M=Rh. For M=Ir, an ordered AFM state at low Cd concentration and a subsequent evolution of the Néel temperature up to 3.8 K is found. This confirms the trend observed for the 115 compounds that the Cd doping favors AFM ordering in these series and suggests that Cd is acting as an electronic tuning agent changing the local density of states that acts fundamentally on the GS behavior. However, there exist experimental evidences that Cd doping is affecting the tetragonal CEF parameters in these compounds. This is reflected in the tendency of the ordered moment to rotate to the ab plane in Cd-doped samples. An evolution of the CEF scheme may also help to understand the behavior of T_{MAX} that increases as a function of Cd concentration. The increase in this parameter is not expected in a scenario where Cd is just acting as an electronic tuning agent. Further experiments such as inelastic neutron scattering should be performed aiming to clarify the function of the Cd doping in the microscopic behavior on these systems. The XRMS and NMS experiments showed that Cd-doped $Ce_2(Rh,Ir)In_8$ has a commensurate magnetic order with propagation vector $\vec{\varepsilon}=(\frac{1}{2},\frac{1}{2},0)$ identical to the pure Ce_2RhIn_8 compound, indicating that Cd doping does not alter the sign of the relative magnetic interaction between the neighboring Ce spins, although it increases the magnitude of the average magnetic interaction between them as it can be seen by the increase in the ordered magnetic moment in the Cd-doped compounds.

ACKNOWLEDGMENTS

This work was supported by FAPESP (SP-Brazil), CNPq (Brazil), and CAPES (Brazil). The staff at the ID-20 beam line and BT-9 instrument is gratefully acknowledged for providing an outstanding scientific environment during these experiments.

*cadriano@ifi.unicamp.br

[1] See, for instance, P. Monthoux and G. G. Lonzarich, Phys. Rev. B **59**, 14598 (1999); Hilbert v. Löhneysen, Achim Rosch, Matthias Vojta, and Peter Wölfle, Rev. Mod. Phys., **79**, 1015 (2007); H. Kronmuller and S. Parkin, *Handbook of Magnetism and Advanced Magnetic Materials* (Wiley, New York, 2007), Vol. 1, Part 2.

[2] T. Park, F. Ronning, H. Q. Yuan, M. B. Salamon, R. Movshovich, J. L. Sarrao, and J. D. Thompson, Nature (London) **440**, 65 (2006).

[3] C. Petrovic, P. G. Pagliuso, M. F. Hundley, R. Movshovich, J. L. Sarrao, J. D. Thompson, Z. Fisk, and P. Monthoux, J. Phys.: Condens. Matter **13**, L337 (2001).

[4] P. G. Pagliuso, N. O. Moreno, N. J. Curro, J. D. Thompson, M.

F. Hundley, J. L. Sarrao, Z. Fisk, A. D. Christianson, A. H. Lacerda, and A. L. Cornelius, Phys. Rev. B **66**, 054433 (2002).
[5] P. G. Pagliuso, R. Movshovich, A. D. Bianchi, M. Nicklas, N. O. Moreno, J. D. Thompson, M. F. Hundley, J. L. Sarrao, and Z. Fisk, Physica B **312-313**, 129 (2002).
[6] G.-Q. Zheng, N. Yamaguchi, H. Kan, Y. Kitaoka, J. L. Sarrao, P. G. Pagliuso, N. O. Moreno, and J. D. Thompson, Phys. Rev. B **70**, 014511 (2004).
[7] T. Park, V. A. Sidorov, F. Ronning, J.-X. Zhu, Y. Tokiwa, H. Lee, E. D. Bauer, R. Movshovich, J. L. Sarrao, and J. D. Thompson, Nature (London) **456**, 366 (2008).
[8] M. Nicklas, V. A. Sidorov, H. A. Borges, P. G. Pagliuso, C. Petrovic, Z. Fisk, J. L. Sarrao, and J. D. Thompson, Phys. Rev. B **67**, 020506(R) (2003).
[9] L. Mendonça-Ferreira, T. Park, V. Sidorov, M. Nicklas, E. M. Bittar, R. Lora-Serrano, E. N. Hering, S. M. Ramos, M. B. Fontes, E. Baggio-Saitovich, H. Lee, J. L. Sarrao, J. D. Thompson, and P. G. Pagliuso, Phys. Rev. Lett. **101**, 017005 (2008).
[10] E. D. Bauer, F. Ronning, C. Capan, M. J. Graf, D. Vandervelde, H. Q. Yuan, M. B. Salamon, D. J. Mixson, N. O. Moreno, S. R. Brown, J. D. Thompson, R. Movshovich, M. F. Hundley, J. L. Sarrao, P. G. Pagliuso, and S. M. Kauzlarich, Phys. Rev. B **73**, 245109 (2006).
[11] S. M. Ramos, M. B. Fontes, A. D. Alvarenga, E. Baggio-Saitovitch, P. G. Pagliuso, E. D. Bauer, J. D. Thompson, J. L. Sarrao, and M. A. Continentino, Physica B **359-361**, 398 (2005).
[12] M. Daniel, E. D. Bauer, S.-W. Han, C. H. Booth, A. L. Cornelius, P. G. Pagliuso, and J. L. Sarrao, Phys. Rev. Lett. **95**, 016406 (2005).
[13] L. D. Pham, T. Park, S. Maquilon, J. D. Thompson, and Z. Fisk, Phys. Rev. Lett. **97**, 056404 (2006).
[14] M. Nicklas, O. Stockert, T. Park, K. Habicht, K. Kiefer, L. D. Pham, J. D. Thompson, Z. Fisk, and F. Steglich, Phys. Rev. B **76**, 052401 (2007).
[15] R. R. Urbano, B.-L. Young, N. J. Curro, J. D. Thompson, L. D. Pham, and Z. Fisk, Phys. Rev. Lett. **99**, 146402 (2007).
[16] J. G. Donath, F. Steglish, E. D. Bauer, F. Ronning, J. L. Sarrao, and P. Gegenwar, EPL **87**, 57011 (2009).
[17] E. N. Hering, H. A. Borges, S. M. Ramos, M. B. Fontes, E. Baggio-Saitovich, E. M. Bittar, L. Mendonça Ferreira, R. Lora-Serrano, C. Adriano, P. G. Pagliuso, J. L. Sarrao, and J. D. Thompson, Physica B **403**, 780 (2008).
[18] N. O. Moreno, M. F. Hundley, P. G. Pagliuso, R. Movshovich, M. Nicklas, J. D. Thompson, J. L. Sarrao, and Z. Fisk, Physica B **312-313**, 274 (2002).
[19] D. Kaczorowski, A. P. Pikul, D. Gnida, and V. H. Tran, Phys. Rev. Lett. **103**, 027003 (2009); K. Uhlírová, J. Prokleška, and V. Sechovský, *ibid.* **104**, 059701 (2010).
[20] W. Bao, P. G. Pagliuso, J. L. Sarrao, J. D. Thompson, Z. Fisk, and J. W. Lynn, Phys. Rev. B **64**, 020401(R) (2001).
[21] G. D. Morris, R. H. Heffner, N. O. Moreno, P. G. Pagliuso, J. L. Sarrao, S. R. Dunsiger, G. J. Nieuwenhuys, D. E. MacLaughlin, and O. O. Bernal, Phys. Rev. B **69**, 214415 (2004).
[22] P. G. Pagliuso, J. D. Thompson, M. F. Hundley, J. L. Sarrao, and Z. Fisk, Phys. Rev. B **63**, 054426 (2001).
[23] Z. Fisk and J. P. Remeika, *Handbook on the Physics and Chemistry of Rare Earths* (Elsevier, North-Holland, Amsterdam, 1989), Vol. 12, p. 53.
[24] P. G. Pagliuso, J. D. Thompson, M. F. Hundley, and J. L. Sarrao, Phys. Rev. B **62**, 12266 (2000).
[25] P. G. Pagliuso, D. J. Garcia, E. Miranda, E. Granado, R. Lora Serrano, C. Giles, J. G. S. Duque, R. R. Urbano, C. Rettori, J. D. Thompson, M. F. Hundley, and J. L. Sarrao, J. Appl. Phys. **99**, 08P703 (2006).
[26] R. Lora-Serrano, C. Giles, E. Granado, D. J. Garcia, E. Miranda, O. Agüero, L. Mendonça-Ferreira, J. G. S. Duque, and P. G. Pagliuso, Phys. Rev. B **74**, 214404 (2006).
[27] N. V. Hieu, H. Shishido, H. Nakashima, K. Sugiyama, R. Settai, T. Takeuchi, T. D. Matsuda, Y. Haga, M. Hagiwara, K. Kindo, and Y. Onuki, J. Magn. Magn. Mater. **310**, 1721 (2007).
[28] J. Hudis, R. Hu, C. L. Broholm, V. F. Mitrović, and C. Petrovic, J. Magn. Magn. Mater. **307**, 301 (2006).
[29] S. Doniach, in *Valence Instabilities and Related Narrow Band Phenomena*, edited by R. D. Parks (Plenum, New York, 1977), p. 169.
[30] E. G. Moshopoulou, Z. Fisk, J. L. Sarrao, and J. D. Thompson, J. Solid State Chem. **158**, 25 (2001).
[31] E. G. Moshopoulou, R. M. Ibberson, J. L. Sarrao, J. D. Thompson, and Z. Fisk, Acta Crystallogr., Sect. B: Struct. Sci. **62**, 173 (2006).
[32] C. Adriano, C. Giles, L. Mendonça-Ferreira, F. de Bergevin, C. Mazzoli, L. Paolasini, Z. Fisk, and P. G. Pagliuso, Physica B **404**, 3014 (2009).
[33] J. P. Hill and D. F. McMorrow, Acta Crystallogr., Sect. A: Found. Crystallogr. **A52**, 236 (1996).
[34] M. Blume and D. Gibbs, Phys. Rev. B **37**, 1779 (1988).
[35] C. Adriano, R. Lora-Serrano, C. Giles, F. de Bergevin, J. C. Lang, G. Srajer, C. Mazzoli, L. Paolasini, and P. G. Pagliuso, Phys. Rev. B **76**, 104515 (2007).
[36] E. Granado, P. G. Pagliuso, C. Giles, R. Lora-Serrano, F. Yokaichiya, and J. L. Sarrao, Phys. Rev. B **69**, 144411 (2004).
[37] D. Mannix, P. C. de Camargo, C. Giles, A. J. A. de Oliveira, F. Yokaichiya, and C. Vettier, Eur. Phys. J. B **20**, 19 (2001).
[38] C. Adriano, C. Giles, L. N. Coelho, G. A. Faria, and P. G. Pagliuso, Physica B **404**, 3289 (2009).
[39] G. L. Squires, *Introduction to the Theory of Thermal Neutron Scattering* (Dover, Mineola, New York, 1996).
[40] G. Shirane, S. M. Shapiro, and J. M. Tranquada, *Neutron Scattering with a Triple-Axis Spectrometer: Basic Techniques* (Cambrige University Press, Cambridge, 2002).
[41] M. Blume, A. J. Freeman, and R. E. Watson, J. Chem. Phys. **37**, 1245 (1962).